Natural and Applied Sciences International Journal (NASIJ)
eISSN: 2788-4619 (online)
https://doi.org/10.47264/idea.nasij/3.1.2
Vol. 3, No. 1, (January-June 2022), 13-33
https://www.ideapublishers.org/index.php/nasij Research Article

Wavelet analysis based VTEC variability over mid-latitude region Sukkur, Pakistan and its comparison with IRI models during 2019-2020

Rasim Shahzad*[1] | Amna Hafeez[1] | José Francisco de Oliveira-Júnior[2] | Arslan Ahmed[3] | Punyawi Jamjareegulgarn[4] | Najam Abbas Naqvi[1]

1. Department of Space Sciences, Space Education and GNSS Lab, National Centre of GIS and Space Application, Institute of Space Technology (IST), Islamabad, Pakistan.
2. Engineering School, Postgraduate Program in Biosystems Engineering, Federal University Fluminense (UFF), Niterói, Rio De Janeiro, Brazil.
3. Department of Electrical Engineering, National Skills University, Islamabad, Pakistan.
4. King Mongkut's Institute of Technology Ladkrabang, Prince of Chumphon Campus, Chumphon, Thailand.

***** Corresponding Author Email: rasishaz007@gmail.com

Received: January 16, 2022 Accepted: May 30, 2022 Published: June 30, 2022

Abstract: The Total Electron Content (TEC) from the Sukkur GPS station is studied during the final phase of the solar cycle 24 and the initial phase of solar cycle 25 (2019-2020). TEC comparisons are made with three international reference ionospheric models: IRI-2007, IRI-2012 and IRI-2016. The finding of the study indicates that IRI-2016 is better than IRI-2007 and IRI-2012 in monthly values using wavelet transformation. Moreover, the seasonal variations between observed and modelled VTEC were observed maximum during the spring season. Similarly, the IRI-2016 exhibited maximum correlation (i.e., $r > 0.8$) as compared to the other two models for both solar cycle phases. This study also includes a cross-correlation of GPS-VTEC with several storm indices (Kp, Dst, Ap) via wavelet transformation. In this paper, the wavelet spectrum is analysed for two-year data (2019-2020) to visualize the impact of geomagnetic storm indices on VTEC. Storms of different intensities during 2019-2020 solar activity were also analysed, where maximum correlation from wavelet transformation between GPS VTEC and geomagnetic indices was recorded during the initial solar phase of cycle 25. These kinds of studies assist to correct the measured GPS VTEC and help to improve predicted VTEC over mid-latitude regions.

Keywords: VTEC, GPS, IRI models, wavelet transformation, geomagnetic storms, ionosphere, mid-latitude.

How to Cite: Shahzad, R., Hafeez, A., Oliveira-Júnior, J. F. D., Ahmed, A., Jamjareegulgarn, P., & Naqvi, N. A. (2022). Wavelet analysis based VTEC variability over mid-latitude region Sukkur, Pakistan and its comparison with IRI models during 2019-2020. *Natural and Applied Sciences International Journal (NASIJ), 3*(1), 13-33. https://doi.org/10.47264/idea.nasij/3.1.2

1. Introduction

About 60-1000 Km above the surface of the Earth, an ionized layer called the ionosphere exists having a considerable quantity of ions and free electrons generated as a result of a process known as photoionization (Bilitza, 1986). When ultraviolet and X-ray reaches neutral particles, photoionization occurs (Tariq *et al.*, 2019; 2020). The density of a columnar number of electrons incorporated between two points corresponds to TEC, which is descriptive amount for the ionosphere of the Earth (Mehmood *et al.*, 2021).

The free electrons in the ionosphere cause the time delay in signal propagation. The magnitude of the ionosphere's phase advance or group delay on satellite radio transmission increases with the TEC enhancement but is inversely proportional to the frequency square (Shahzad *et al.*, 2021). The ionosphere has a dispersive structure, due to which GPS signals which are electromagnetic signals, suffer time delay and advancement in modulated codes and carrier phase, respectively while passing and hence receivers placed on grounds may not get signals on listed time (Ioannides & Strangeways, 2000).

The GPS has been utilized around the world as the measurements attained by GPS receiver are proved significant in the assessment of TEC and its variability in the ionosphere (Rahman, 2020; Hussain & Shah, 2020). In the absence of measurements, ionospheric models can be used to estimate VTEC, such as IRI models (Tariku, 2019). Such empirical models are recognized for predicting/modelling the values of ionospheric TEC during several solar magnetic active phases (Timoçin *et al.*, 2018). The analysis of TEC variability of the ionosphere in solar quiet and active days is beneficial and shows a significant practicality in single frequency receiver based navigation using satellites and for the range error corrections and time delay (Tariq *et al.*, 2020).

These models offer comprehensive material about ionospheric physics. TEC from the IRI is acquired by numerically integrating from 50-2000 Km in 1 Km steps. In 1978, the model was first presented (Rawer *et al.*, 1978) and for peak parameters Comité Consultatif International des Radio (CCIR) communications maps are being used that allows global coverage. The IRI models have improved in performance for estimating foF2 over time by updating temperature models (Bilitza, 1986). Moreover, USRI maps have been used (Bilitza, 1990), new selections in D-region integration have been made for topside density of electrons (Bilitza 2001), and new options for storm-time model and auroral boundaries have been added (Araujo-Pradere *et al.*, 2002).

Several studies have been reported about model predicted VTEC and measured VTEC over different latitudes to validate improvements in delay over low and mid-latitude (Chakraborty *et al.*, 2014; Tariku, 2016; Natali & Meza, 2017; Tariq *et al.*, 2020). In mid-latitude, IRI models provide fine observations (Kumar *et al.* 2015; Gordiyenko & Yakovets, 2017; Tariku, 2019; Shahzad *et al.*, 2021).

Furthermore, an ionospheric deviation in the geomagnetic storms can also be relative to the quiet time, as they are the principal cause of the ionospheric variations close to solar cycle phases. Such plasma transport is infatuated with electric field disturbances, winds and thermospheric temperature referring to magnetosphere–ionosphere–thermosphere (M–I–T) interactions. Geomagnetic storms primarily characterize instabilities in the system of M-I-T coupling. The drop in the highest density of electrons in the F2 layer describes the negative ionospheric phase of the storm, while an increase in the F2 layer's top density is used to describe the positive phase of the storm, resulting in the complexity of disruptions seen during geomagnetic storms. This tendency results in TEC variations from the Global Navigation Satellite System (GNSS), which labels TEC as a relatively straightforward metric to measure (Dow *et al.*,2009; Jin *et al.*, 2017). The electron density changes beyond climatological levels during an ionospheric storm are primarily caused by mid-latitude, electric fields and thermospheric winds. The storm time characteristics are primarily characterized by significant VTEC enhancement or depletion.

Electric fields and thermospheric winds are considered as major motives for storms, causing variations in electron density. Hence, such changes are perceived as substantial enhancement or diminution in VTEC features of storm patterns at mid-latitudes (Cander, 2016). Diurnal, monthly and seasonal variations in the ionosphere illustrate its dynamic nature; solar and geomagnetic variability is another inquisitiveness. At low latitude regions, the undervalued pattern of TEC retrieved from IRI models was stated and during unusual solar activity, the irregularities of the TEC from the dense layer in the upper atmosphere at mid-latitudes were also reported by Coïsson and Radicella (2005) and Coïsson *et al.* (2008). In support with the view of better TEC estimated values in the mid-latitude region, Gordiyenko and Yakovets (2017) testified model IRI-2012 and proposed the mechanism of diurnal and seasonal variability at low solar activity times for foF2, which is the critical frequency and hmF2 which is peak density monthly medians height.

Deviations in the values of VTEC retrieved using the IRI model and VTEC of GPS are insignificant, referring to better performance in mid-latitude region reported by Kumar *et al.* (2015). There is no significant research to estimate the pattern of variations at mid-latitude between GPS TEC and modelled TEC during maximum solar phase using recent versions of IRI models i.e. IRI-2007, 2012 and 2016. However, Shahzad *et al.* (2021) reported variation behaviour of these models during a geomagnetically active period. An empirical ionospheric correction model, STORM, is used for geomagnetic activity dependence.

To evaluate diurnal and seasonal variation patterns of VTEC, several types of research have been attempted for different regions by using measured and modelled VTEC values. Such analyses show the night-time VTEC is lower than daytime, while the observed highest VTEC values are about the time of noon and values observed during solstices are lower than equinox season (Bhuyan & Borah 2007; Kumar *et al.*, 2015; Mukesh *et al.*, 2018; Shahzad *et al.*, 2021). The underestimation of model VTEC from IRI-2007 during the ascending period of solar cycle

during 2009–2011 was determined when compared with Kenya's measured GPS during this period (Olwendo *et al.,* 2013). IRI-2012 showed an abnormal deviation of values when compared with GPS measured values of the ionosphere in 2014 over the ZONG station of Turkey, hence raising the seasonal variation possibility (Inyurt *et al.*, 2017). Observations at low latitudes indicate that model IRI-2016 underestimates VTEC values due to Equatorial Ionization Anomaly (EIA), active solar conditions and geomagnetic instabilities (Shi et al., 2018).

The ionosphere produces the largest amount of error in GNSS navigation signals. In mid latitude these errors are quite severe during various conditions. In this layer, TEC exhibits spatial as well as temporal variations. This affects the predicted TEC accuracy of multiple models. But which version of IRI model is most suitable for the mid-latitude region and how much it is accurate? The currently operating dual-frequency Global Positioning System (GPS) receiver in Sukkur, Pakistan is the only station in the country to provide an opportunity to analyze Total Electron Content (TEC) over the mid-latitude region in the most dynamic layer of Earth, ionosphere. In this paper, the behaviour of GPS measured VTEC is analyzed and evaluated with different IRI models during solar cycle 24 final phase and initial phase of solar cycle 25 at mid-latitude zone of Pakistan (Sukkur) for the period of 2019-2020. During solar activity, the geomagnetic indices are correlated with VTEC retrieved from GPS for identifying the possible variable behaviour. For this purpose, GPS retrieved VTEC and IRI modelled VTEC for quiet and disturbed days is analyzed to study the different features of ionospheric data.

This research will benefit the improvement and correction of ionospheric scintillation in the Sukkur region. Furthermore, detecting abnormalities in the mid-latitude ionosphere will aid in the improvement of characteristics undergoing GPS ionospheric adjustments for communication and navigation solutions. Ionospheric plasma density in these regions validates a substantial variability in the VTEC of the ionosphere encompassing latitude, longitude, time of day, season and geomagnetically active times.

This paper is organized as follows: Section 2 explains the data and methods used to analyze the TEC behaviour and accuracy of IRI models over mid-latitude regions. Section 3 comprehensively explains results and discussions and also describes various conditions under which GPS TEC and IRI model predicted TEC behaviour is monitored. The paper conclusions are summarized in section 4, unfolding main findings of the study and providing answer to the question about the accuracy of different models in mid-latitude region.

2. Methodology

The Sukkur region in Pakistan, a mid-latitude region with a Geographic Latitude 27.7° N, Longitude 68.8° E and Geomagnetic Dipole of 19.97° N, was the location of the dual frequency GNSS receiver utilized in this study to obtain GPS-TEC data (Figure 1). This study compares

the retrieved VTEC from various models and calculated GPS VTEC from Sukkur Station for the 2019–2020 period. A useful way to depict, evaluate, and explain the overall conduct of the near-Earth thermal plasma is to use the complete ionospheric electron thickness profile to obtain VTEC (Froń *et al.*, 2020; Shahzad *et al.*, 2021).

The Slant TEC (STEC) is obtained using a Septentrio Polarx5S multi-frequency GNSS receiver and is available in Ionospheric Scintillation Monitoring Records (ISMR). STEC can be obtained along the view line between the transmitter and the ground station. It is measured in terms of the number of free electrons per square meter in the unit of TECU (1 TECU equals 10^{16} electrons/m2). The IONOLAB software is used to calculate the STEC (Arikan *et al.*, 2003; 2008). In which, TEC estimates are provided with a 30s resolution for both active and non-active solar conditions for all stations in various latitudes, using the Regularized Estimation (Reg-Est) Algorithm. Furthermore, it refers to GIM-TEC maps from IGS as a reference for biases. The following equations can be used to determine the STEC in a square meter region using the dual frequency GPS receiver:

$$\text{STEC} = \frac{f_1^2 f_2^2}{40.28\left(f_1^2 - f_2^2\right)}\left(L_1 - L_2 + \lambda_1(N_1 + b_1) - \lambda_2(N_2 + b_2) + \epsilon\right) \quad \ldots\ldots\ldots\ldots\ldots\ldots\ldots\ldots\ldots\ldots \quad (1)$$

$$\text{STEC} = \frac{f_1^2 f_2^2}{40.28\left(f_1^2 - f_2^2\right)}\left(P_1 - P_2 - (d_1 - d_2) + \epsilon\right) \quad \ldots\ldots\ldots\ldots\ldots\ldots\ldots\ldots\ldots\ldots\ldots\ldots\ldots\ldots\ldots\ldots \quad (2)$$

In the above equations, f_1 and f_2 represent the carrier phase frequency at both ends. Moreover, pseudo-range and the delay path of the signal of carrier phase observations are denoted as L and P respectively. Signal wavelength is represented as λ and ray path uncertainty as N. Biases of consequent signal pseudo-range and instrument's carrier phase are represented as d and b, and random remainder in signal is ϵ. Following is the equation for STEC to VTEC conversion (Heki & Enomoto, 2013; Shah *et al.*, 2020; Hussain & Shah, 2020).

$$\text{VTEC} = \text{STEC} \times \cos\left(arcsine\left(\frac{RsinZ}{R+H}\right)\right) \quad \ldots\ldots\ldots\ldots\ldots\ldots\ldots\ldots\ldots\ldots\ldots\ldots\ldots\ldots\ldots\ldots\ldots\ldots \quad (3)$$

Where, Z is the elevation angle of satellite for point of observation. Moreover, R and H represents earth's radius and ionosphere height, respectively (Klobuchar, 1987).

To check the long-term behaviour of computed VTEC, correlation was made with different geomagnetic indices including Ap, Kp and Dst(nT) retrieved from https://omniweb.gsfc.nasa.gov/form/dx1.html using wavelet coherence cross-spectrum. A wavelet having a zero mean is localized function in time and space. Characterization of wavelet can be done based on its localization in time and frequency. Measurement of correlation among two-time series is called wavelet correlation and can be computed using the following equation (Grinsted *et al.*, 2004; Li & He, 2017).

Figure 1: (a) Red star shows the GNSS station of Sukkur (Latitude 27.7° N, Longitude 68.8° E) (b) GNSS antenna of Sukkur Station (c) Sukkur Station Septentrio Polarx5S receiver with background working

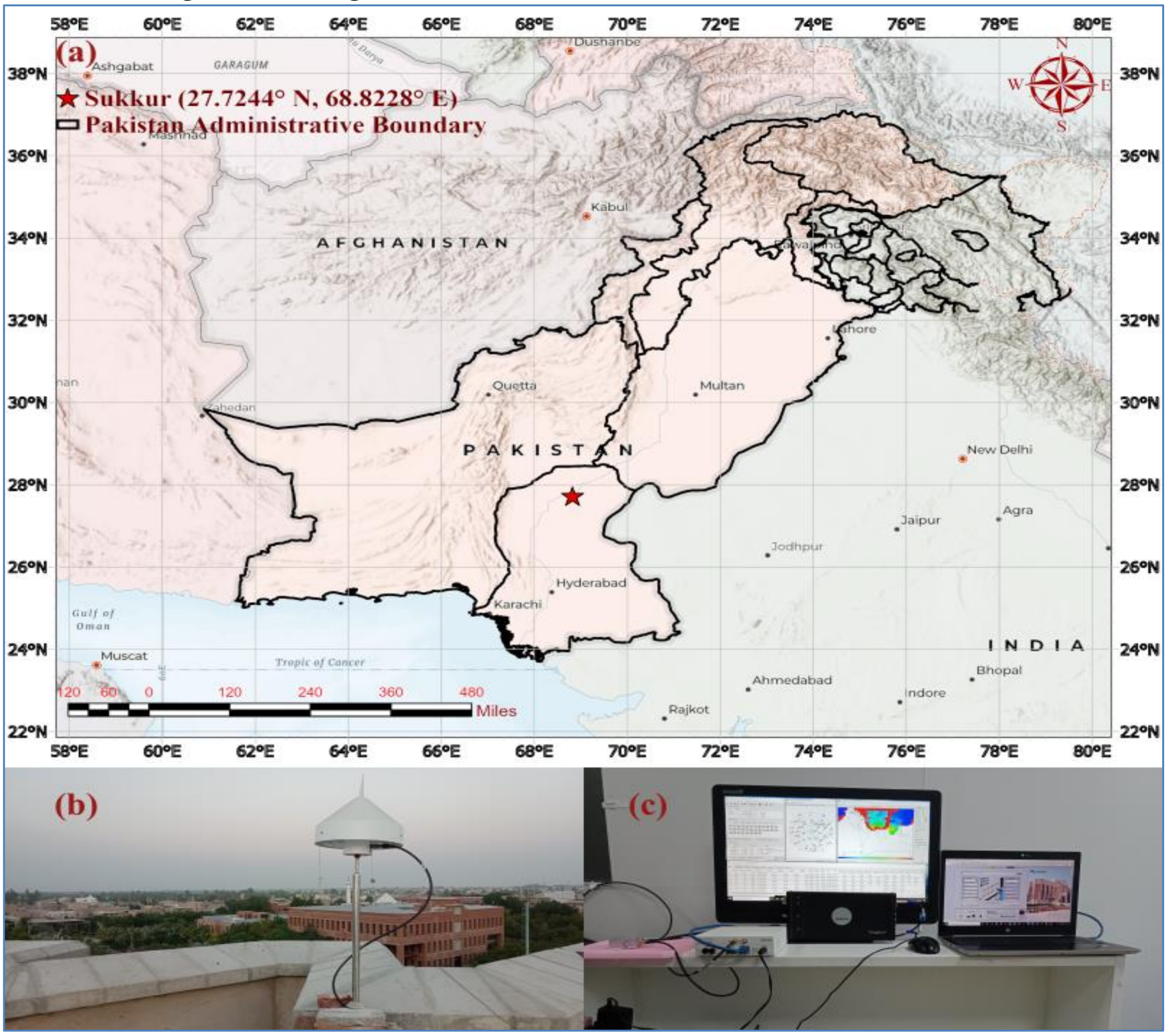

$$R_n^2(s) = \frac{\left|S\left(s^{-1}W_n^{XY}(s)\right)\right|^2}{S\left(s^{-1}\left|W_n^X(s)\right|^2 \cdot S\left(s^{-1}\left|W_n^Y(s)\right|^2\right)\right)} \quad \text{..........} \quad (4)$$

Where, S represents the smoothing operator in scale and time and at different positions and scales. The continuous wavelet transformation of two time series is represented as $W_n^X(s)$ and $W_n^Y(s)$. In a time, frequency space wavelet coherence is a localized correlation coefficient. Equation for smoothing operator (S) is:

$$S(W) = S_{scale}(S_{time}(W_n(s))) \quad \text{..........} \quad (5)$$

Where S_{time}, S_{scale} represents the smoothing in time and smoothing along the wavelet scale axis respectively. Smoothing operators design depends upon the basis of its similarity with

wavelet footprint (Guedes *et al.*, 2015). The coherence Morlet wavelet is preferred for the smoothing operator in below equations.

$$S_{time}(W)|s = \left(W_n(s) * \ c1^{\frac{-t^2}{2s^2}}\right) \qquad (6)$$

$$S_{time}(W)|s = (W_n(s) * c2\Pi(0.6s))|n \qquad (7)$$

Where rectangle function is Π and normalization constants are denoted as *c1* and *c2*. Scale decorrelation length for the Morlet wavelet is determined empirically to be 0.6. The measure of power distribution is the wavelet cross-spectrum between two time series (X, Y), and it may be calculated using the formulae stated in Torrence and Compo's (1998) article. The wavelet cross spectrum of the x and y time series:

$$= S(W_n^{X*}(s)W_n^{Y}(s)) \qquad (8)$$

Where continues wavelet transformation of two time series X and Y is denoted as $W_n^X(s)$ and $W_n^Y(s)$ at different scales and positions. Smoothing operator in scale and time is denoted as S and superscript * represents the complex conjugate.

The NeQuick option was selected for IRI models for the density of electron at topside in order to achieve IRI TEC. IRI-2007 chose B0Table for the bottom side thickness, while IRI-2012 and IRI-2016 chose (ABT-2009). Additionally, IRI-2007 (TTSA-2000), IRI-2012 (TBT-2012 and IRI-2016 (TBT2012 + SA) were chosen for the parameter Topside Te. Additionally, during IRI-2007, IRI-2012 and IRI-2016, the ion compositions were (DS95/TTS05), (RBV10/TTS03) and (RBV10/TBT15) respectively. Additionally, the F2 peak density was calculated by means of the URSI option and the storm model of F-peak was turned off for every model. Further information on the model, whose values in this inquiry are compared to the observation, can be examined (https://ccmc.gsfc.nasa.gov/).

In order to analyse the diurnal VTEC variability, one magnetically calm day was observed and for monthly analysis, one quiet day was chosen from each month. The GPS VTEC for the period 2019–2020 was received GPS station installed at Sukkur and VTEC of IRI model was built from IRI models provided by CCMC. Particularly to observe seasonal behaviour, the diurnal readings for the chosen non-active solar days were summed and averaged for every season to observe the fluctuations in VTEC.

As illustrated below, the model retrived VTEC is subtracted from the measured VTEC using GPS receiver to calculate the diurnal VTEC variations.

$$dTEC = IRI\,VTEC - GPS\,VTEC \qquad (9)$$

The following equation is used to determine Percent Deviation (PD), which is used to observe the model's capacity.

$$PD = \frac{IRITEC_i - GPSTEC_i}{GPSTEC_i} \times 100 \quad \ldots\ldots (10)$$

Where, $GPSTEC_i$ represents measured values and $IRITEC_i$ displays modelled values. The following equation is used to calculate the correlation coefficient for assessing how well the IRI model VTEC and GPS VTEC agree (Tariq *et al.*, 2019).

$$\text{Correlation Coefficient} = \frac{\sum_i (\text{GPSTEC}_i - \overline{\text{GPSTEC}_i})(IRITEC_i - \overline{IRITEC_i})}{\sqrt{\sum_i (\text{GPSTEC}_i - \overline{\text{GPSTEC}_i})^2}\sqrt{\sum_i (IRITEC_i - \overline{IRITEC_i})^2}} \quad \ldots\ldots (11)$$

Where, $GPSTEC_i$ is the observed VTEC data of GPS receiver at Sukkur station, $\overline{GPSTEC_i}$ is their mean, $IRITEC_i$ is the modelled VTEC data retrieved from CCMC using various IRI models, and $\overline{IRITEC_i}$ is IRI measure VTEC mean (see Table-1).

Table-1: Comparison of GPS and IRI model VTEC

Period		Correlation Coefficient					
		2019			2020		
Models		IRI-2007	IRI-2012	IRI-2016	IRI-2007	IRI-2012	IRI-2016
Monthly	Jan	0.766	0.802	0.975	0.583	0.581	0.812
	Feb	0.959	0.969	0.813	0.739	0.704	0.834
	Mar	0.881	0.924	0.925	0.773	0.786	0.851
	Apr	0.782	0.8610	0.958	0.855	0.846	0.881
	May	0.923	.970	0.987	0.960	0.943	0.918
	Jun	0.773	0.727	0.732	0.906	0.866	0.856
	Jul	0.990	0.979	0.988	0.868	0.831	0.860
	Aug	0.956	0.985	0.998	0.936	0.902	0.872
	Sep	0.885	0.923	0.996	0.740	0.798	0.822
	Oct	0.842	0.880	0.998	0.877	0.854	0.812
	Nov	0.848	0.870	0.993	0.913	0.922	0.923
	Dec	0.855	0.862	0.994	0.824	0.832	0.946
Seasonal	Winter	0.959	0.969	0.813	0.844	0.818	0.630
	Spring	0.782	0.861	0.958	0.915	0.925	0.918
	Summer Solstice	0.773	0.727	0.732	0.780	0.775	0.789
	Equinox	0.885	0.923	0.996	0.872	0.846	0.778

3. Results and discussions

In this paper, GPS measured VTEC from Sukkur GPS Station is compared with the IRI model retrieved VTEC during non-active days in 2019-2020 in monthly and seasonal analysis. The core objective of this study is to correct the dispersive behaviour of ionosphere over mid-

latitude Pakistan. Moreover, we compared the VTEC values with geomagnetic indices of long-term data over the mid-latitude Pakistani region and carried out their correlation pattern. The detail of all result is described below.

3.1. Monthly variations

To examine the variability of VTEC for long-term data of 2019-2020, we chose one quiet day of each month and compared these values with IRI-predicted VTEC (Figure 2). IRI-2007 provided minimum deviation during June and December throughout the day for 2019 (Figure 2b), as well as 2020 (Figure 2d); whereas similar pattern was also observed for IRI-2012. Moreover, maximum deviation of 48.4 TECU and 54.1 TECU was also observed during January and February for IRI-2012 during 2019 and 2020, respectively (Figure 2b & 2d).

Figure 2: Depiction of monthly quite days variation of GPS measured VTEC of Sukkur station as comparison to IRI models from 2019 to 2020, where (a) represents VTEC variation and its comparison with IRI models (2007, 2012 and 2016) in Solar cycle 24 final phase (b) shows deviation of IRI-2007 (yellow area), IRI-2012 (orange area) and IRI-2016 (blue area) from GPS measured VTEC during year 2019 (c) illustrate GPS measured VTEC comparison with IRI models in initial phase of Solar cycle 25 (d) shows deviation of IRI-2007 (yellow area), IRI-2012 (red area) and IRI-2016 (blue area) from GPS measured VTEC during year 2020.

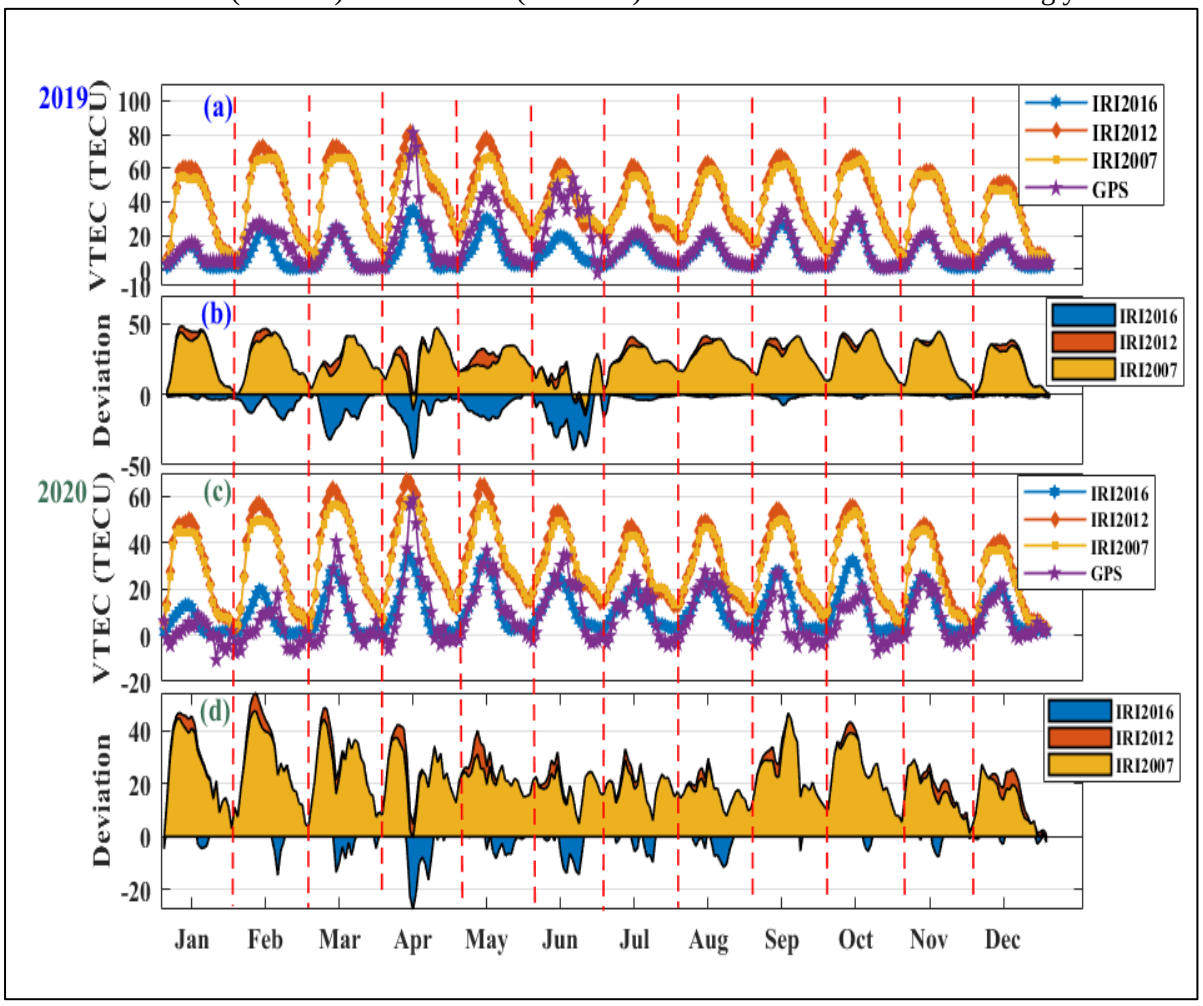

The model IRI-2016 presented high deviation during March, April and June out of which April depicted the peak value of 27.4 TECU during 2020 and 45.5 TECU during 2019 and low values were recorded for January, August, November and December (Figure 2a & 2b). For the year 2020, IRI 2016 also variate the lowest values during similar months i.e., January, November and December. The pattern of maximum deviated values showed approximately double the values during 2019 as compared to 2020 (Figure 2c & 2d).

The GPS VTEC deviation is higher from the IRI-2007 and the IRI-2012 predicted VTEC, because above 2,000 Km, the plasmaspheric electron content density exists and both of these empirical models are not capable of contemplating the plasmaspheric component (Ezquer *et al.*, 2018). For the mid-latitude region, Shahzad *et al.* (2021) also noted a similar pattern of greater VTEC between March and April and a less deviation in the month of November and December.

Additionally, Inyurt *et al.* (2017) proposed that VTEC reach its peak around April. Ionospheric abnormalities over the Sukkur region for the months of April and May are suggestively stronger than the rest of the months on strong Equatorial Electrojet (EEJ) days as a result of the spread of EIA crest to mid latitude regions. As Sukkur lies in mid-latitude region, it undergoes greater EIA expansion which is produced by increased EEJ over the region in the form of upward drifts due to higher electric field causing more inconsistency during these months (Matamba *et al.*, 2016; Shahzad *et al.*, 2021).

3.2. Seasonal variations

3.2.1. Winter season

During winter season, IRI-2007 predicted higher VTEC values during 2019 (Figure 3a) as compared to year 2020 (Figure 3c) by giving 44.3 TECU deviation from GPS observed VTEC. This minimum deviation was occurred on UTC 2200 hours to 2400 hours during 2019-2020 (Figures 3b & 3d). The VTEC predicted by the IRI-2012 model throughout the year 2019 winter season and between UTC 0500 and 1400 hours were higher than the GPS measured VTEC values. We noted the maximum deviation between these values (37-47 TECU) (Figure 3b).

In 2020, the maximum deviation of 53 TECU was observed, which is 7 TECU higher than the peak deviation attained during 2019 at UTC=0700 hours (Figure 3d). Similarly, during winter season, the maximum deviation of 10-18 TECU was observed at UTC 1300-1800 hours and UTC 0700-0900 hours during 2019-2020. During 2019, a peak deviation of 18.3 TECU of 3% more deviation than the maximum deviation in 2020. Overall, the GPS observed VTEC mean values detected for winter season is higher in 2019. Similarly, IRI predicted mean VTEC values are higher during 2020 (Figure 4a & 4b).

3.2.2. Spring season

For the year 2019, two IRI models (IRI 2007 and IRI 2012) predicted VTEC is nearly equal, resulting in a maximum deviation of 35TECU-48TECU from GPS VTEC at UTC 1200hours-1900hours whereas at UTC 0700 hours-1400 hours the maximum deviation of 33TECU-44TECU was observed during year 2020 (Figure 3a & 3d). During 2019 and 2020, however, the minimum variation was recorded at UTC 0900 hours to 1100 hours and UTC 2300 hours to 2400 hours respectively (Figure 3b & 3d). During 2019, the IRI modelled mean values (2007 & 2012) generally overstated the GPS recorded VTEC values (Figure 4a). For the year 2019, the IRI 2016 modelled mean VTEC underestimated the GPS VTEC whereas, the modelled VTEC for the year 2020 overestimated the GPS VTEC (Figure 4a & 4b). In comparison to the other seasons of the year, this model showed the most variance during the spring season of 2019.

3.2.3. Summer solstice

Overall, during this season IRI-2016 modelled values underestimated GPS VTEC for both years i.e., 2019 and 2020 whereas the overestimated GPS VTEC were observed by IRI-2012 and IRI-2007 (Figure 3a & 3c). The peak deviation was recorded at UTC 2100 hours and UTC 0800 hours by IRI-2007 and IRI-2012 during 2019 and 2020, respectively. The minimal values of deviation were listed during UTC 1300 hours to 1600 hours ranging between 2-7 TECU for both years. However, the IRI-2016 predicted VTEC showed maximum deviation at the UTC 1300 hours and minimum of 2-6 TECU during UTC 2000 hours to 2400 hours (Figure 3b & 3d).

3.2.4. Equinox

The GPS measured the VTEC value was underestimated by IRI 2007 and IRI 2012 throughout the day during 2019 as well as 2020, the maximum deviation ranged between 30-40TECU and the minimum deviation was observed to range between 2-10TECU during UTC 2300 hours-2400 hours (Figure 3). The minimum deviation was observed throughout the day during both years for IRI 2016 model and maximum deviation of 7.5TECU at UTC 0900 hours was observed during 2019 while 15.6TECU at UTC 0800 hours was listed during 2020 (Figure 3b & 3d).

Tariq et al. (2020) and Shehzad et al. (2021) also comprehended that the seasonal mean VTEC is minimal among GPS measured and the IRI-2016 retrieved the VTEC on comparison with other models during all seasons. Similar findings were confirmed by Arikan et al. (2007) while examining VTEC data from eight GPS sites (Trabzon, Nicosia, Ankara, Istanbul, Gebze, Ohrid, Sofia and Zelenchukskaya). Additionally, findings of our study were in agreement with the seasonal VTEC data from the Turkish station studies (Inyurt et al., 2017; Ansari et al., 2017; 2018).

Figure 3: Represent seasonal comparison between modelled VTEC of IRI models retrieved and GPS measured VTEC during final phase and initial phase of Solare cycles 24 and 25 respectively, where (a) represents seasonal variation of measured GPS VTEC (purple line) and its comparison with IRI-2007 (yellow line), IRI-2012 (orange line) and IRI-2016 (blue line) during year 2019 (b) shows deviancy between model's retrieved VTEC and calculated VTEC using GPS Solar cycle 24 final phase (c) illustrate seasonal variation of GPS measured VTEC during 2020 and its comparison with IRI models (d) shows deviation of IRI-2007 (yellow area), IRI-2012 (orange area) and IRI-2016 (blue area) form GPS measured VTEC during year 2020

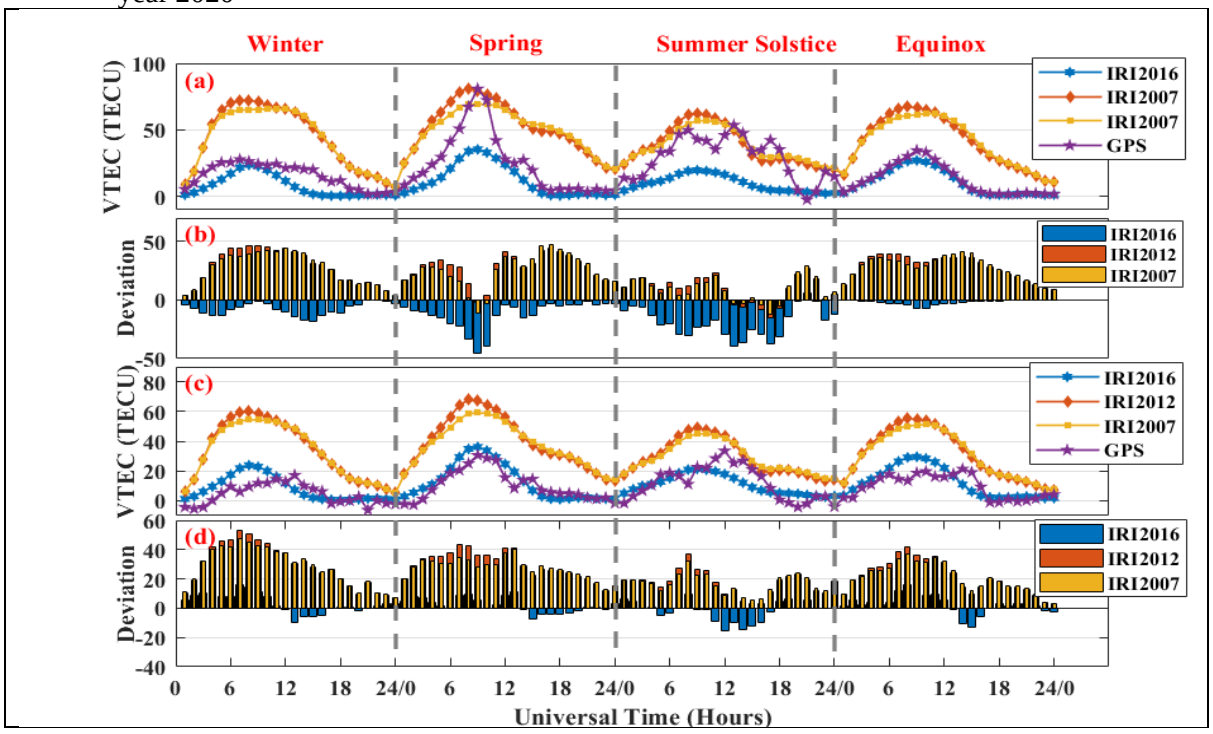

Figure 4: Seasonal deviation of GPS measured mean VTEC and its evaluation with IRI models (2007, 2012 and 2016), where (a) mean VTEC comparison between GPS measured VTEC and IRI models VTEC during Solar cycle 24 final phase (b) represents mean GPS measured VTEC comparison with different IRI models

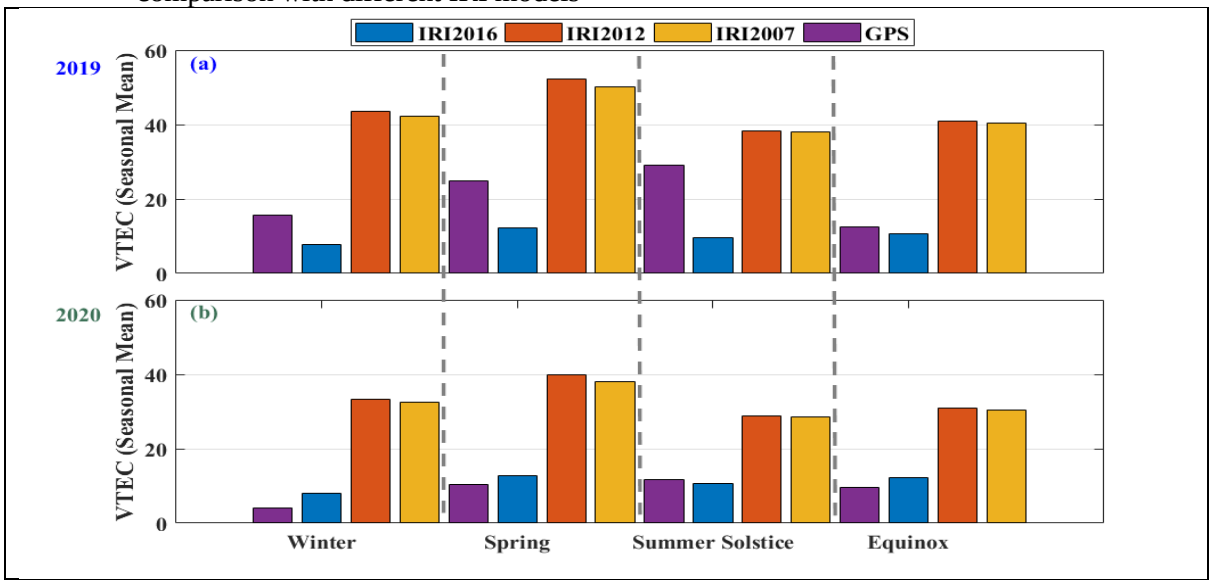

Correlation coefficient (*r*) is computed to evaluate the agreement between IRI models retrieved VTEC and measured GPS VTEC (Figure 5). In 2019 and 2020, there is a noteworthy correlation among IRI-2016 and GPS-measured VTEC >8 for both seasonal and monthly values (Figure 5c, 5f, 5i & 5l). While IRI-2007 depicted minimum correlation with GPS measured VTEC <0.7 during final phase of Solar cycle 24 for both seasonal and monthly analysis (Figure 5a, 5d, 5g & 5j).

Whereas, IRI-2012 showed correlation value between 0.7 to 0.8 for both years seasons and monthly analysis (Figure 5b, 5e, 5h & 5k). For quiet days throughout their investigation of total electron content, Tariku (2019) and Sharma *et al*. (2018) reported comparable results. The variance among IRI models and GPS VTEC is produced by variations in the concentration of electrons owing to photo-ionization brought on by the recombination or transport process (Wu *et al.*, 2004).

Figure 5: Correlation graphs of GPS and IRI VTEC where (a-f) represents seasonal correlation between GPS VTEC and IRI models (2007, 2012 and 2016) VTEC during 2019 and 2020 and (g-l) shows monthly correlation between calculated VTEC of GPS station and IRI modelled VTEC for both years (2019 and 2020)

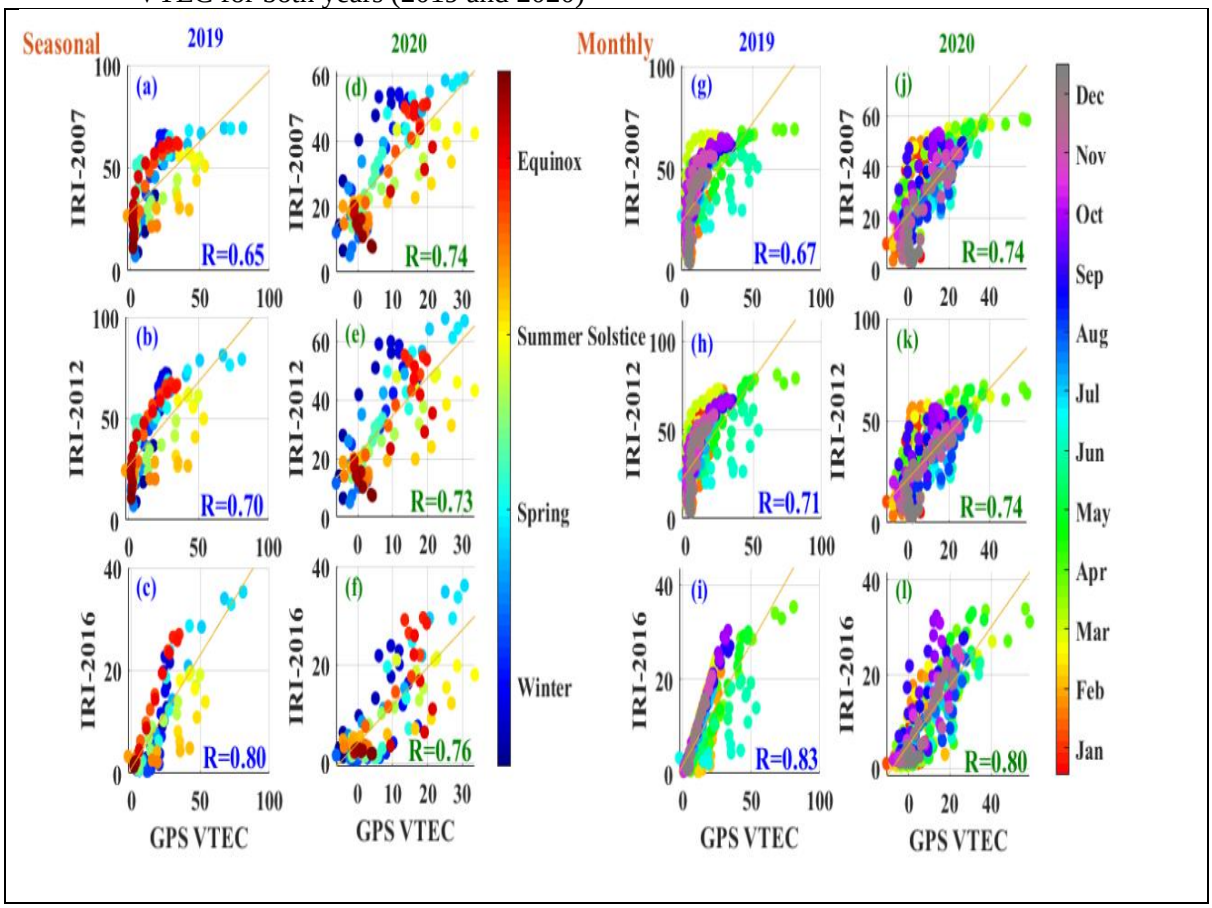

3.3. Geomagnetic storm indices correlation with GPS VTEC

To analyse dynamics of ionosphere and its global structure the GPS technique is being widely

used. The geomagnetic perturbations induce strong changes in the ionosphere. Many research groups have used GPS receiver and numerous methods of estimating TEC to monitor TEC on global as well as regional scale (Bhawre *et al.*, 2011). By using ionospheric TEC calculated by means of GPS receiver at the location of Sukkur region this study demonstrates TEC response to geomagnetic storm. These responses involve amplitude changes and TEC variability on daily basis has been monitored. Particularly at middle latitude, TEC respond substantially to geomagnetic storms, this kind of study is also reported by (Aa *et al.*, 2018; Shim *et al.*, 2018). However, TEC changes may result in a deterioration of the GNSS signal and reduced location accuracy in the impacted area.

Our analysis includes a few magnetically active periods during 2019 and 2020 over mid-latitude Sukkur region (Figure 6). Typically, to describe geomagnetic activity level there are two indices being used, i.e. the A index and the K index**.** These indices provide idea of the magnetic fluctuations' severity and thus ionosphere perturbations. This paper proposes a novel approach where ionospheric VTEC is correlated with different Geomagnetic storm indices such as Kp, Ap and DsT by using wavelet coherence cross spectrum technique.

Figure 6: Represents GPS measured VTEC variation as compared to Geomagnetic indices, where (a) show Dst (nT) indices variation from 2019 to 2012 depicting different storms conditions (b) illustrate Kp indices variation during 2019 and 2020 showing different ranges for various storm conditions (c) represents Ap indices behaviour throughout the 2 years2019-2020) with different storm conditions (d) shows GPS measured VTEC response as compared to Dst (nT), Ap and Kp indices during final phase of Solar cycle 24 and initial phase of Solar cycle of 25

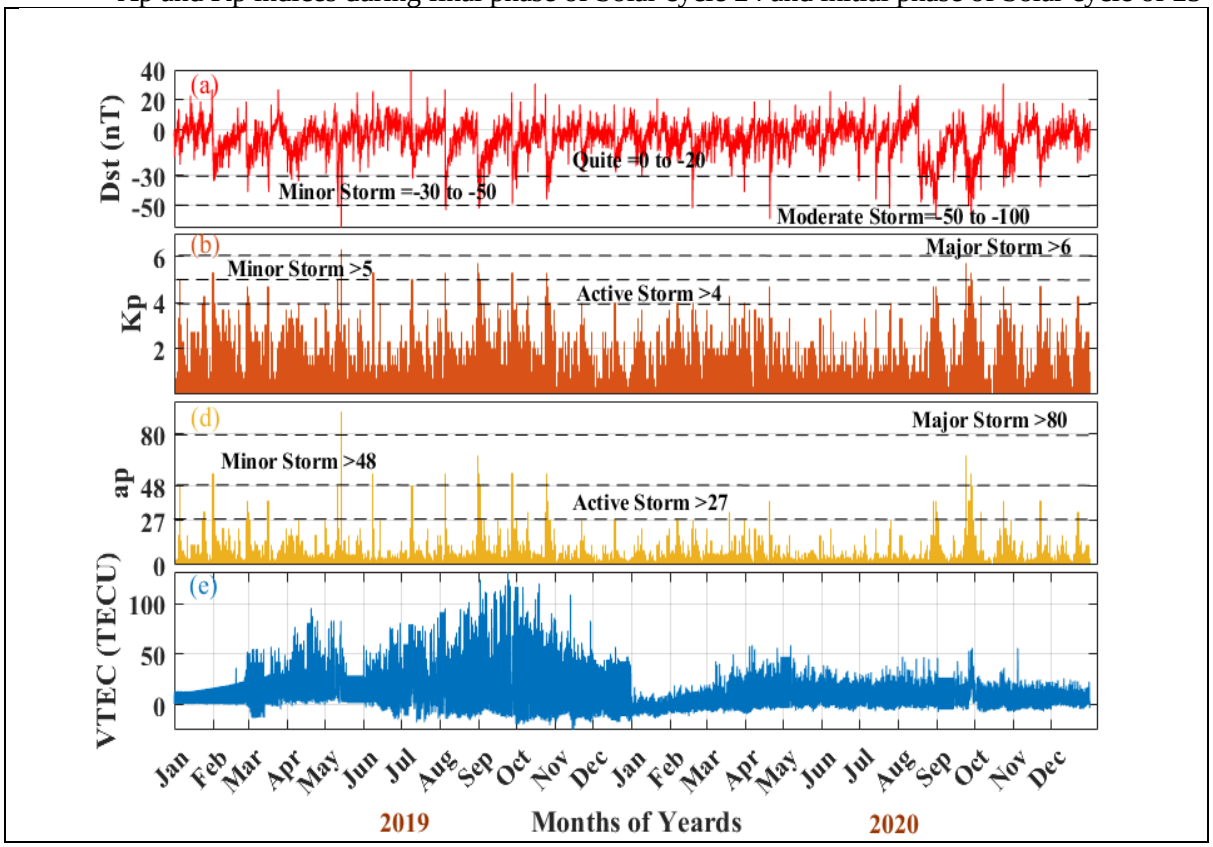

For minor storm of Ap (48-80) the cross correlation obtained between GPS VTEC and Ap index value was >0.7 in the month of February, 2019 than later in the same year at the end of May a major storm (>80) was observed which gave correlation of >0.8 (Figure 7). The minor storm was observed during the month of October of year 2020 which also showed peak value of cross correlation (>0.9) between two-time series (Figure 7c).

Figure 7: Represents wavelet coherence between GPS measured VTEC and Ap indices during year 2019 and 2020 (a) shows GPS measured VTEC from 2019 to 2020 (b) illustrate Ap indices variation during both years (2019 and 2020) (c) represents wavelet coherence cross spectrum along with magnitude squared coherence to show the extent of correlation between GPS measured VTEC and Ap indices during final and initial phase of Solar cycle 24, 25 respectively.

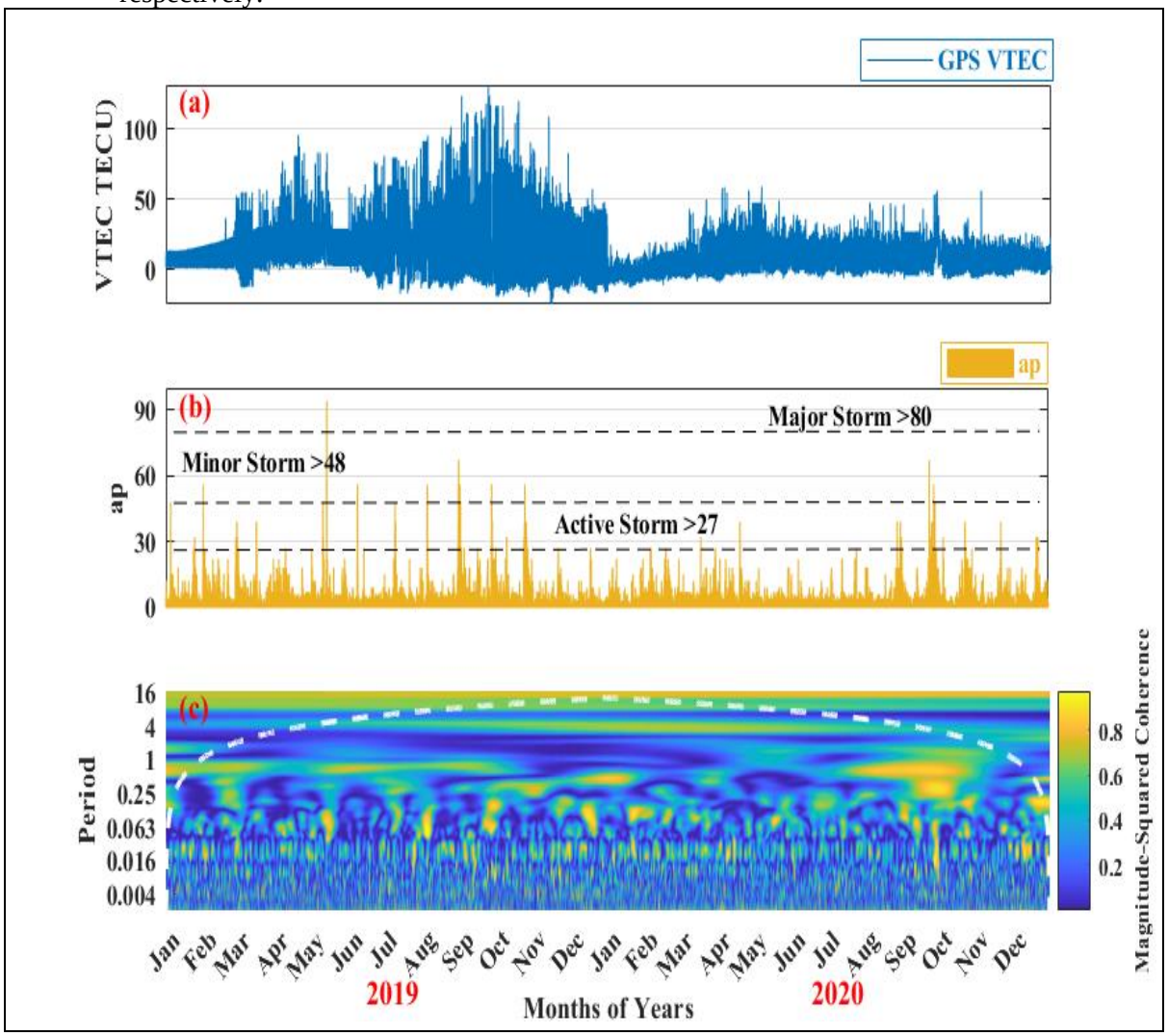

While analysing Kp index maximum value of cross correlation was attained during October of both years (2019 & 2020) (Figure 8). The major storm was observed at the end of May, 2019 where correlation value was 0.8 (Figure 8b & 8c). During 2020 the wavelet cross-coherence spectrum illustrated that correlation was attained for longer span i.e., from July to October (Figure 8c).

Figure 8: Represents wavelet coherence between GPS measured VTEC and Kp indices during final phase of Solar cycle 24 and initial phase of Solar cycle 25 (2019-2020) where (a) shows GPS measured VTEC variation during 2019 and 2020 (b) illustrate Kp variation from 2019 to 2020 (c) represents correlation between GPS measured VTEC and Kp indices during final and initial phase of Solar cycle 24, 25 respectively using wavelet coherence cross spectrum along with magnitude squared coherence

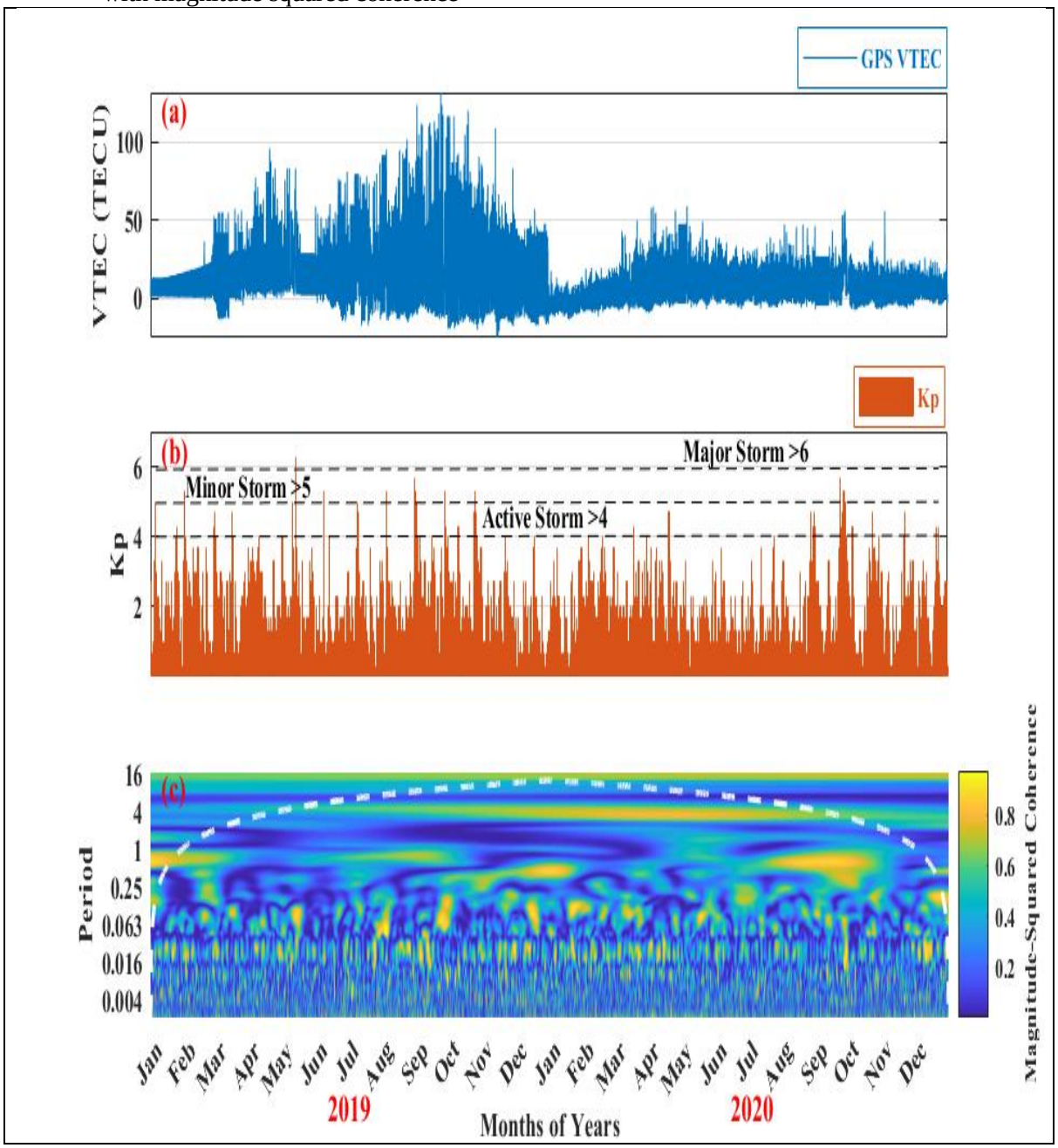

When the GPS VTEC and Dst index were analysed (Figure 9), we observed a moderate storm in May, 2019 where VTEC values fluctuated accordingly (Figure 9b). The maximum correlation of >0.9 was showed in August, 2019 followed by 0.6-0.7 correlation in the later months. Overall, the maximum correlation of >0.9 was attained during September and October of year 2020 (Figure 9c).

Figure 9: Represents wavelet coherence between GPS measured VTEC and Dst indices for long term data (2019 to 2020) where, (a) shows GPS measured VTEC variation during final phase of Solar cycle 24 and initial phase of Solar cycle 25 (b) illustrated Dst indices variation from 2019 to 2020 (c) represents wavelet coherence (correlation) cross spectrum along with magnitude squared coherence between GPS measured VTEC and Dst indices from 2019 to 2020

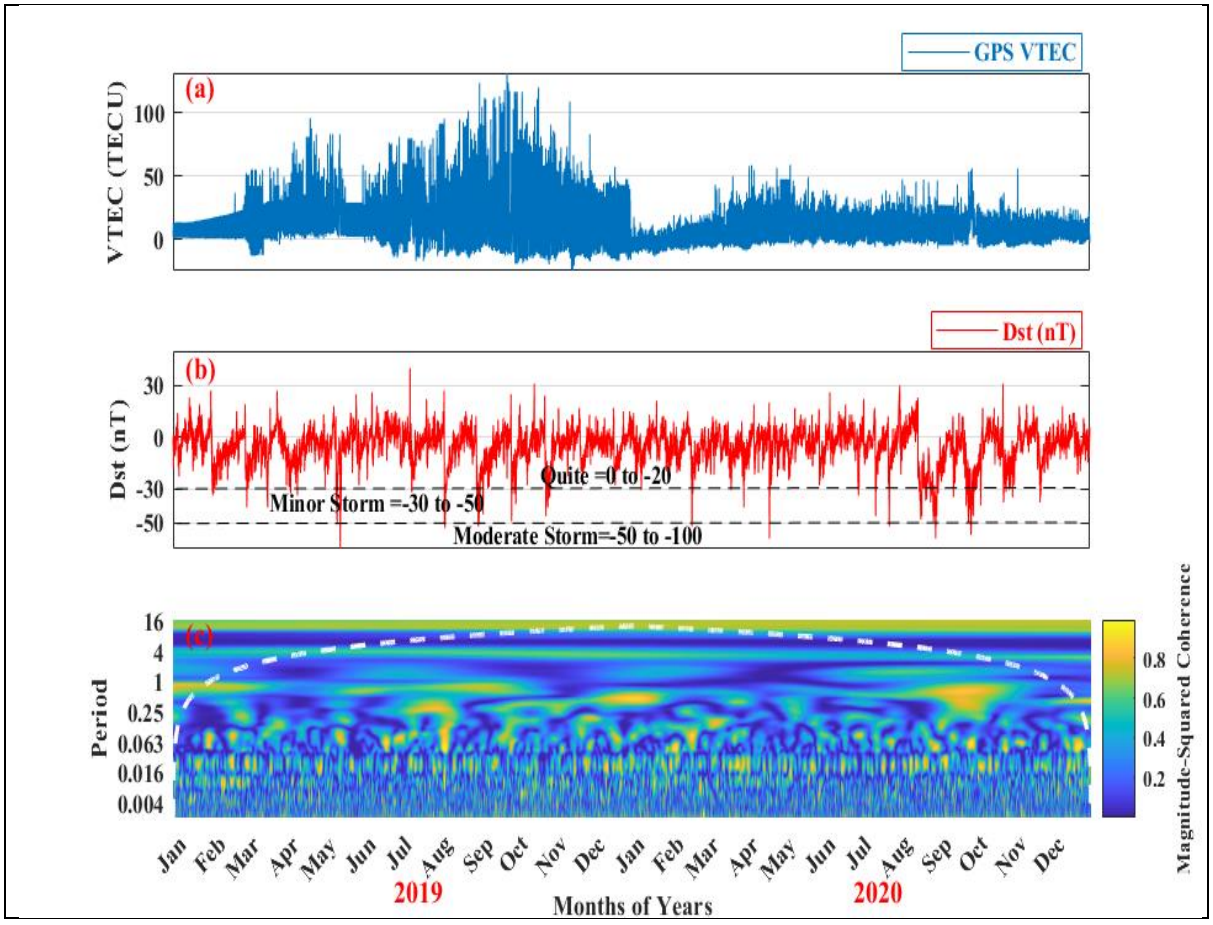

4. Conclusion

The geomagnetic field's distinct geometry in Pakistan's mid-latitude region exhibits significant impact on radio waves propagating through the ionosphere. The possible variabilities in GPS VTEC are analysed with in situ IRI model values to corroborate the perturbed behaviour in our station measurements. For providing better approximation for monthly and seasonal VTEC IRI-2016 it is the best performing model. Good agreement between the GPS VTEC and the VTEC retrieved from IRI-2016 is observed in monthly analysis. Values from August, October, and December were highly correlated. However, the largest deviations were seen in June and April. Seasonal variation revealed a strong link between GPS VTEC and IRI-2016. The hypothesis that IRI-2016 values were better associated to GPS values with least variability during the investigation came from the comparison of IRI models with GPS VTEC. Furthermore, GPS measured VTEC showed good correlation with geomagnetic storm indices during major (correlation > 0.9) and moderate (correlation > 0.8) storms. Good correlation was also attained during initial phase of solar cycle 25 for longer period as compared to Solar cycle 24 last phase. However, further studies should be carried out to analyse VTEC variability over mid latitude regions to comprehend its deviation from modelled VTEC.

Acknowledgement

The authors are grateful to OMNI Web NASA and CCMC for making the data for IRI models and storm indices available. The authors appreciate Sukkur, IBA for providing the GPS VTEC data as well.

References

Aa, E., Huang, W., Liu, S., Ridley, A., Zou, S., Shi, L., Chen, Y., Shen, H., Yuan, T., Li, J., & Wang, T. (2018). Midlatitude plasma bubbles over China and adjacent areas during a magnetic storm on 8 September 2017. *Space Weather, 16*(3), 321–331. https://doi.org/10.1002/2017SW001776

Ansari, K., Panda, S. K., Althuwaynee, O. F., & Corumluoglu, O. (2017). Ionospheric TEC from the Turkish Permanent GNSS Network (TPGN) and comparison with ARMA and IRI models. *Astrophysics and Space Science, 362*(9), 178. https://doi.org/10.1007/s10509-017-3159-z

Ansari, K., Panda, S. K., & Corumluoglu, O. (2018). Mathematical Modelling of Ionosperic TEC from Turkis permanent GNSS Network (TPGN) Observables during 2009–2017 and predictability of NeQuick and Kriging models. *Astrophysics and Space Science, 363*(42), 1-13. https://doi.org/10.1007/s10509-018-3261-x

Araujo-Pradere, E. A., Fuller-Rowell, T. J., & Codrescu, M. V. (2002). TORM: An empirical storm-time ionospheric correction model 1. Model description. *Radio Sciences, 37*(5), 1070. https://doi.org/10.1029/2001RS002467

Arikan, F., Erol, C, B., & Arikan, O. (2003). Regularized estimation of vertical total electron content from Global Positioning System data. *Journal of Geophysical Research Atmospheres, 108*(A12). https://doi.org/10.1029/2002JA009605

Arikan, F., Arikan, O., & Erol, C.B. (2007). Regularized estimation of TEC from GPS data for certain midlatitude stations and comparison with the IRI model. *Advances in Space Research. 39*(5), 867-874. https://doi.org/10.1016/j.asr.2007.01.082.

Arikan, F., Nayir, H., Sezen, U., & Arikan, O. (2008). Estimation of single station interfrequency receiver bias using GPS-TEC. *Radio Science, 43*(4),1-13. https://doi.org/10.1029/2007RS003785.

Belehaki, A., Jakowski, N., & Reinisch, B. (2003). Comparison of ionospheric ionization measurements over Athens using ground ionosonde and GPS derived TEC values. *Radio Sciences*., 38(6), 1105. https://ieeexplore.ieee.org/abstract/document/7770735/

Bhawre, D. P., Purushottam, Mansoori, A. A., & Yadav, R. (2011). The response of polar, equatorial and low latitude ionosphere to the minor magnetic disturbance of 11 October 2008. *International Journal of Engineering Science and Technology, 3*(1).

Bhuyan, P. K., & Borah, R. R. (2007). TEC derived from GPS network in India and comparison with the IRI. *Advances in Space Research, 39*(5), 830-840. https://doi.org/10.1016/j.asr.2006.12.042

Bilitza, D. (1986). International reference ionosphere: Recent developments. *Radio Science, 21*(3), 343-346. https://doi.org/10.1029/RS021i003p00343Citations.

Bilitza, D. (1990). *International reference ionosphere 1990*. Science Applications Research Lanham Maryland, USA. https://ntrs.nasa.gov/api/citations/19910021307/downloads/19910021307.pdf

Bilitza, D. (2001). International reference ionosphere 2000. *Radio Science, 36*(2), 261–275. https://doi.org/10.1029/2000RS002432

Cander, L. R. (2016). Re-visit of ionosphere storm morphology with TEC data in the current solar cycle. *Journal of Atmospheric and Solar-Terrestrial Physics*, *138-139*, 187-205. https://doi.org/10.1016/j.jastp.2016.01.008

Chakraborty, M., Kumar, S., Kumar, B., & Guha, A. (2014). Latitudinal characteristics of GPS derived ionospheric TEC: A comparative study with IRI 2012 model. *Annals of Geophysics*, *57*(5), A0539. https://doi.org/ 10.4401/ag-6438

Coïsson, P., & Radicella, S. M. (2005). Ionospheric topside models compared with experimental electron density profiles. *Annals of Geophysics*, *48*(3), 497-503. https://doi.org/ 10.4401/ag-3214.

Coïsson, P., Radicella, S., Nava, B., & Leitinger, R. (2008). Low and equatorial latitudes topside in NeQuick. *Journal of Atmospheric and Solar-Terrestrial Physics, 70*(6), 901–906. https://doi.org/10.1016/j.jastp.2007.05.017

Dow, J. M., Neilan, R. E., & Rizos, C. (2009). The International GNSS Service in a changing landscape of Global Navigation Satellite Systems. *Journal of Geodesy*, *83*, 191-198. https://doi.org/10.1007/s00190-008-0300-3

Ezquer, R.G., Scidá, L. A., Orué, Y. M., Nava, B., Cabrera, M. A., & Brunini, C. (2018). NeQuick 2 and IRI Plas VTEC predictions for low latitude and South American sector. *Advances in Space Research, 61*(7), 1803-1818. https://doi.org/10.1016/j.asr.2017.10.003

Froń, A., Galkin, I., Krankowski, A., Bilitza, D., Hernández-Pajares…& García-Rigo, A. (2020). Towards cooperative global mapping of the ionosphere: Fusion feasibility for IGS and IRI with global climate VTEC map. *Remote Sensing, 12*(21), 3531. https://doi.org/10.3390/rs12213531

Gordiyenko, G. I., & Yakovets, A. F. (2017). Comparison of midlatitude ionospheric F region peak parameters and topside Ne profiles from IRI2012 model prediction with ground-based ionosonde and Alouette II observations. *Advances in Space Research*, *60*(2), 461–474. https://doi.org/10.1016/j.asr.2017.01.006

Grinsted, A., Moore, J. C., & Jevrejeva, S. (2004). Application of the cross wavelet transform and wavelet coherence to geophysical time series. Nonlin. *Processes Geophys*, *11*, 561–566. https://doi.org/10.5194/npg-11-561-2004

Guedes, M. R. G., Pereira, E. S., & Cecatto, J. R. (2015). Wavelet analysis of CME, X-ray flare, and sunspot series. Astronomy & Astrophysics, *573*. https://doi.org/10.1051/0004-6361/201323080

Heki, K., & Enomoto, Y. (2013). Pre seismic ionospheric electron enhancements revisited. *Journal of Geophysical Research: Space Physics, 118*(10), 6618–26. https://doi.org/10.1002/jgra.50578

Hussain, A., & Shah, M. (2020). Comparison of GPS TEC with IRI models of 2007, 2012, and 2016 over Sukkur, Pakistan. *Natural and Applied Sciences International Journal (NASIJ), 1*(1), 1–10. https://doi.org/10.47264/idea.nasij/1.1.1

Inyurt, S., Yildirim, O., Mekik, Ç. (2017). Comparison between IRI-2012 and GPS-TEC observations over the western Black Sea. *Annales Geophysicae, 35*(4), 817–24. https://doi.org/10.5194/angeo-35-817-2017.

Ioannides, R.T., & Strangeways, H. J. (2000). Ionosphere-induced errors in GPS range finding using MQP modelling, ray-tracing and nelder-mead optimization. In *Millennium Conference on Antennas and Propagation Switzerland, 2*, 404–408.

Jin, S., Jin, R., & Kutoglu, H. (2017). Positive and negative ionospheric responses to the March 2015 geomagnetic storm from BDS observations. *Journal of Geodesy*, *91*(6), 613-626. https://link.springer.com/article/10.1007/s00190-016-0988-4

Klobuchar, J. A. (1987). Ionospheric Time-Delay Algorithm for Single-Frequency GPS Users. *IEEE Transactions on Aerospace and Electronic Systems*, *AES-23*(3), 325–31. https://doi.org/10.1109/TAES.1987.310829

Kumar, S., Tan, E. L., & Murti, D. S. (2015). Impacts of solar activity on performance of the IRI-2012 model predictions from low to mid latitudes. *Earth Planets Space, 67*, 42. https://doi.org/10.1186/s40623-015-0205-3

Li, F., & He, L. (2017). The effects of dominant driving forces on summer precipitation during different periods in Beijing. *Atmosphere*, *8*(3), 44. https://doi.org/10.3390/atmos8030044.

Liu, A., Ningho, W., Zishen, L., Zhiyu, W., & Hong, Y. (2019). Assessment of NeQuick and IRI-2016 models during different geomagnetic activities in global scale: Comparison with GPS-TEC, dSTEC, Jason-TEC and GIM. *Advances in Space Ressearch, 63*(12), 3978–3992. https://doi.org/10.1016/j.asr.2019.02.032

Matamba, T.M., Habarulema, J.B., & Burešová, D. (2016). Mid latitude ionospheric changes to four great geomagnetic storms of solar cycle 23 in Southern and Northern Hemispheres. *Space Weather, 14*(12), 1155–1171. https://doi.org/10.1002/2016SW001516.

Mehmood, M., Filijar, R., Saleem, S., Shah, M., & Ahmad, A. (2021). TEC derived from local GPS network in Pakistan and comparison with IRI-2016 and IRI-PLAS 2017. *Acta Geophysica, 69*, 381–389. https://doi.org/10.1007/s11600-021-00538-0.

Mosert, M., Gende, M., Brunini, C., Ezquer, R., & Altadill, D. (2007). Comparisons of IRI TEC predictions with GPS and digisonde measurements at Ebro. *Advances in Space Research, 39*, 841–847.

Mukesh, R., Soma, P., Sindhu, P., & Elangovan, R. R. (2018). Comparison of total electron content of IRNSS with IRI and GPS-TEC at equatorial latitude station. *AIP Conference Proceedings 2039*. https://doi.org/10.1063/1.5079004.

Natali, M. P., & Meza, A. (2017). PCA and VTEC climatology at midnight over mid-latitude regions. *Earth Planets and Space, 69*(1). 1399. https://doi.org/10.1186/s40623-017-0757-5

Olwendo, O. J., Baki, P., Cilliers, P. J., Mito, C., & Doherty, P. (2013). Comparison of GPS TEC variations with IRI-2007 TEC prediction at equatorial latitudes during a low solar activity (2009–2011) phase over the Kenyan region. *Advances in Space Research, 52*(10), 1770–79. https://doi.org/10.1016/j.asr.2012.08.001

Rawer, K., Bilitza, D., & Ramakrishan, S. (1978). Goals and status of the International Reference Ionosphere. *Reviews of Geophysics and Space Physics*, *16*(2), 177-181. https://doi.org/10.1029/RG016i002p00177

Rahman, Z. U. (2020). Possible seismo ionospheric anomalies before the 2016 Mw 7.6 Chile earthquake from GPS TEC, GIM TEC and Swarm Satellites. *Natural and Applied Sciences International Journal (NASIJ)*, 1(1), 11–20. https://doi.org/10.47264/idea.nasij/1.1.2

Shahzad, R., Shah, M., & Ahmad, A. (2021). Comparison of VTEC from GPS and IRI-2007, IRI-2012 and IRI-2016 over Sukkur Pakistan. *Astrophysics and Space Science, 366*, 42. https://doi.org/10.1007/s10509-021-03947-1

Sharma, S. K., Ansari, K., & Panda, S. K. (2018). Analysis of ionospheric TEC variation over Manama, Bahrain, and Comparison with IRI-2012 and IRI-2016 Models. *Arabian*

Journal for Science and Engineering, 43, 3823–3830. https://doi.org/10.1007/s13369-018-3128-z.

Shah, M., Aibar, A. G., Tariq, M. A., Ahmed, J., & Ahmed, A. (2020). Possible ionosphere and atmosphere precursory analysis related to Mw > 6.0 earthquakes in Japan. Remote Sensing of Environment, 239, 111620. https://doi.org/10.1016/j.rse.2019.111620

Shim, J. S., Tsagouri, I., Goncharenko, L., Rastaetter, L., Kuznetsova, M., …. & Förster, M., (2018). Validation of ionospheric specifications during geomagnetic storms: TEC and foF2 during the 2013 March storm event. *Space Weather, 16*(11), 1686–1701. https://doi.org/10.1029/2018SW002034

Tariku, Y. A. (2016). The study of variability of TEC over mid-latitude American regions during the ascending phase of solar cycle 24 (2009– 2011). *Advances in Space Research, 58,* 598–608.

Tariku, Y. A., 2019. Testing the improvement of performance of the IRI model in the estimation of TEC over the mid-latitude American regions. *Advances in Space Research, 63*(7), 2066-2074. https://doi.org/10.1016/j.asr.2018.12.009

Tariq, M. A., Shah, M., Ulukavak, M., M., & Iqbal, T. (2019). Comparison of TEC from GPS and IRI-2016 model over different regions of Pakistan during 2015–2017. *Advances in Space Research*, 64, 707-718. https://doi.org/10.1016/j.asr.2019.05.019

Tariq, M. A., Shah, M., Inyurt, S., Shah, M. A., & Liu, L. (2020). Comparison of TEC from IRI-2016 and GPS during the low solar activity over Turkey. *Astrophysics and Space Science*, 365(179). https://doi.org/10.1007/s10509-020-03894-3

Timoçin, E., Ünal, I., & Göker, U. D. (2018). A comparison of IRI-2016 foF2 predictions with the observations at different latitudes during geomagnetic storms. *Geomagnetism and Aeronomy, 58*(7), 846–56. https://doi.org/10.1134/S0016793218070216

Torrence, C., & Compo, G. P. (1998). A practical guide to wavelet analysis. *Bulletin of the American Meteorological society*, *79*(1), 61-78. https://doi.org/10.1175/1520-0477(1998)079%3C0061:APGTWA%3E2.0.CO;2

Wu, C.C., Fry, G., Liu, J.Y., Liou, K., & Tseng, C.L. (2004). Annual TEC variation in the equatorial anomaly region during the solar minimum: September 1996–August 1997. *Journal of Atmospheric and Solar-Terrestrial Physics, 66*(3–4), 199–207. https://doi.org/10.1016/j.jastp.2003.09.017